Supporting Material for

Structural analysis of adenovirus VAI RNA defines the mechanism of inhibition of PKR

Katherine Launer-Felty[1], C. Jason Wong[1], and James L. Cole[1,2*]

[1]Department of Molecular and Cell Biology and [2]Department of Chemistry

University of Connecticut, Storrs, Connecticut 06269, USA

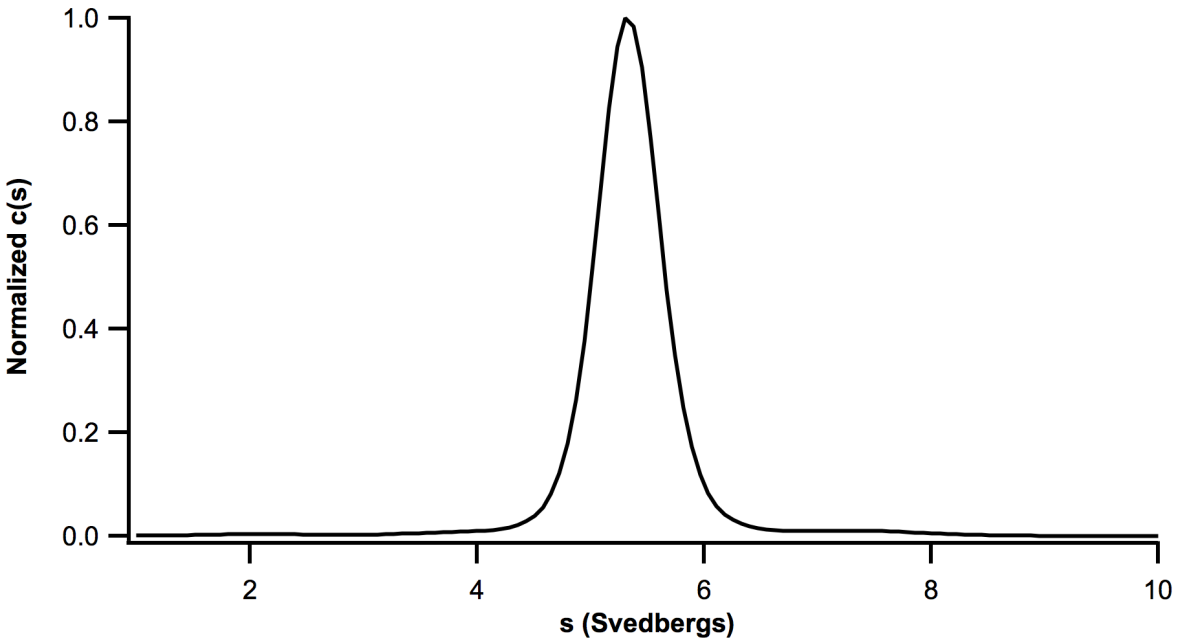

Figure S1. Sedimentation velocity analysis of VAI. VAI was analyzed in AU200 buffer by sedimentation velocity analytical ultracentrifugation. The data were processed using SEDFIT (1) to produce a c(s) distribution. A single species is detected, indicating homogeneity. The peak maximum at ~ 5 S corresponds to the sedimentation coefficient of a VAI monomer (2). Conditions: rotor speed, 35,000 RPM; temperature, 20 °C.

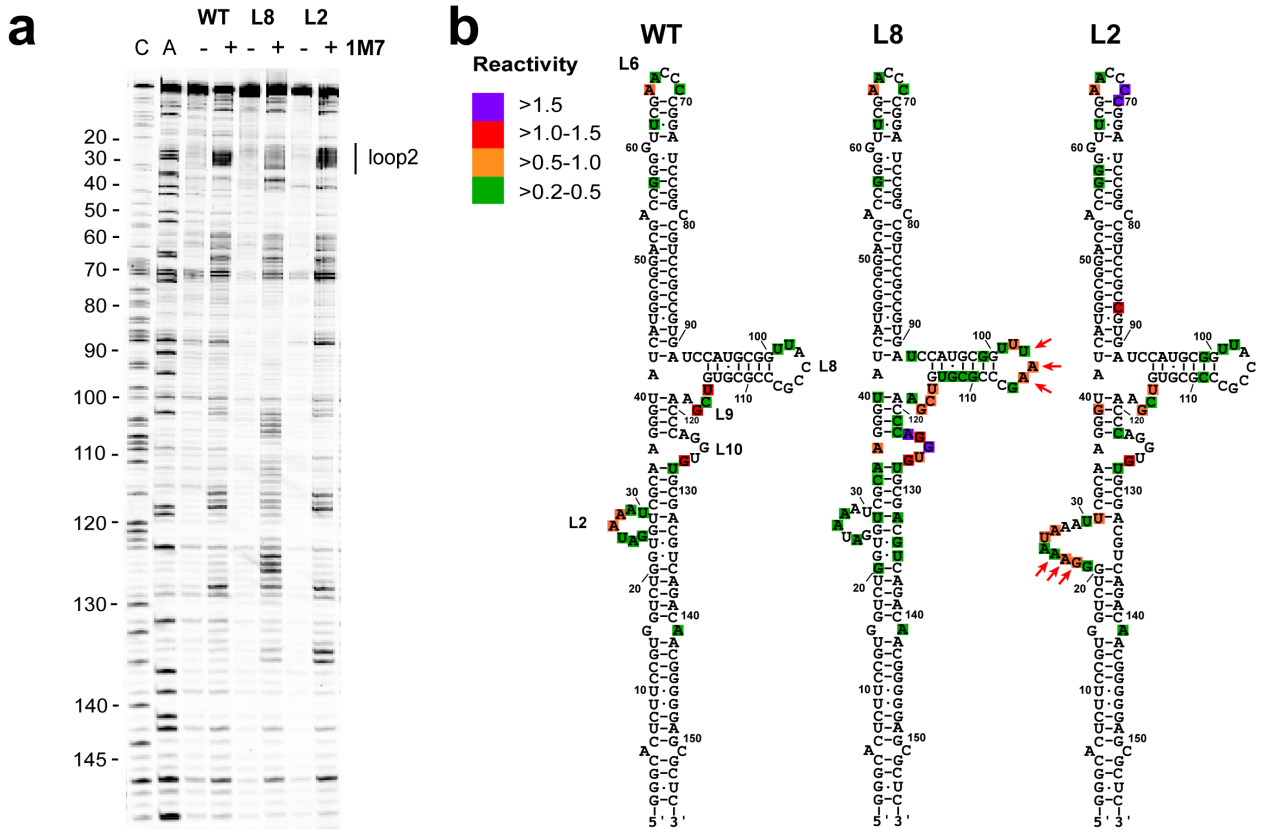

Figure S2. SHAPE analysis of the L2 mutant of VAI. a) SHAPE probing of VAI structure. The gel includes C and A sequencing ladders, a control lane without SHAPE reagent (-) and a lane with 1M7 (+). The L8 mutant is included for comparison. Loop 2 is marked on right side of gel. b) SHAPE reactivity. The locations of the mutations are indicated by red arrows. Reactivities were quantitated using SAFA (3) and normalized to the band corresponding to A65. The reactivities are indicated in color scale indicated in the legend.

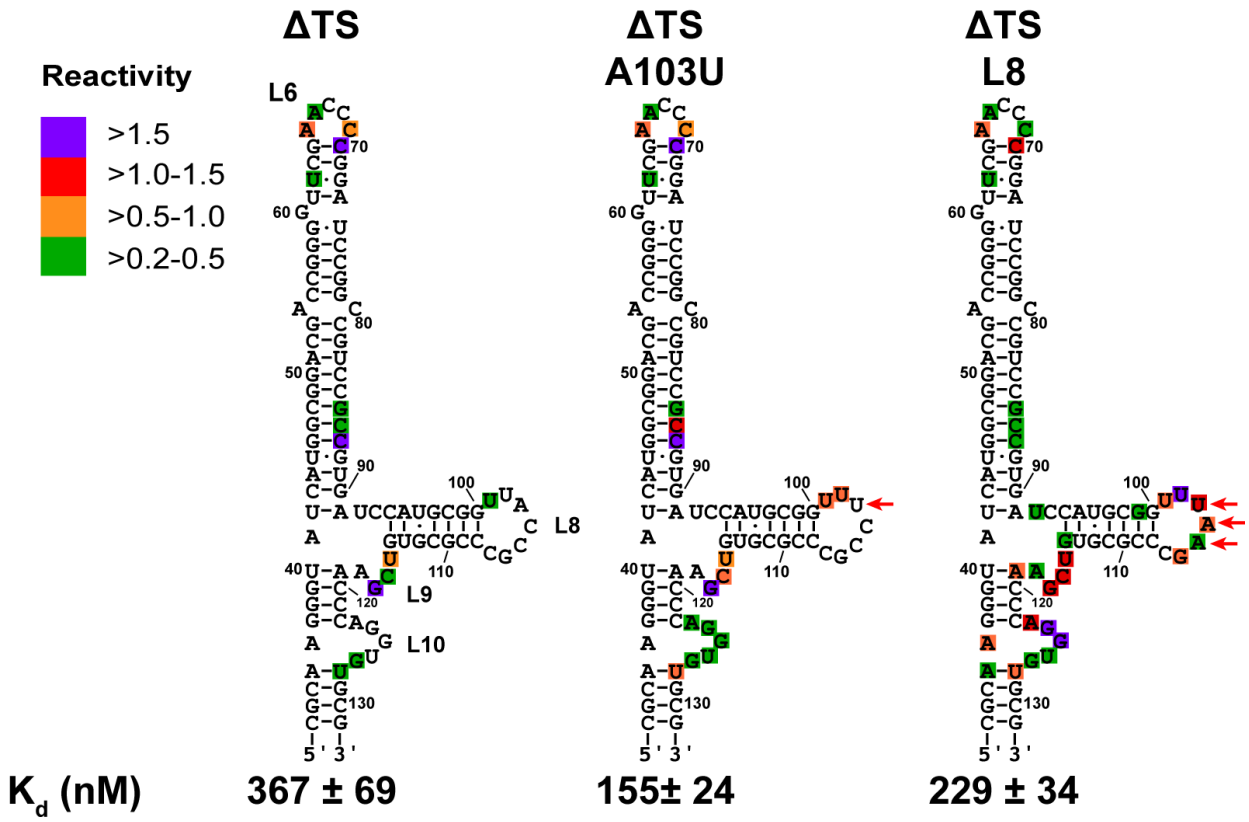

Figure S3. Analysis of ΔTS VAI mutants. The locations of the mutations are indicated by red arrows. The shape reactivities were quantitated using SAFA(3) and normalized to the band corresponding to A65. The reactivities are indicated in color scale indicated in the legend. The dissociation constants for PKR interaction were determined by sedimentation velocity analysis using SEDANAL (4).

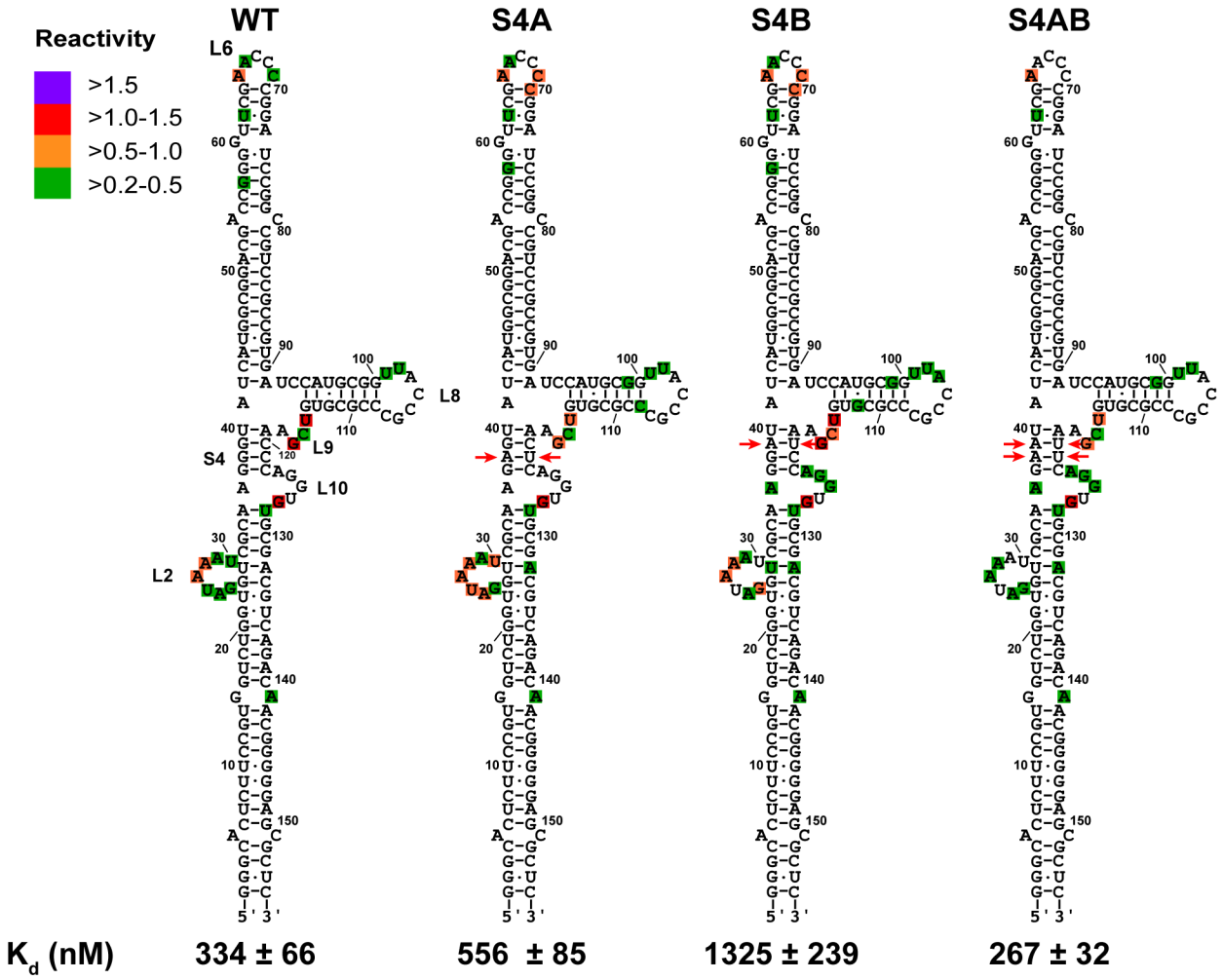

Figure S4. Analysis of stem 4 mutants. The locations of the mutations are indicated by red arrows. The shape reactivities were quantitated using SAFA(3) and normalized to the band corresponding to A65. The reactivities are indicated in color scale indicated in the legend. The dissociation constants for PKR interaction were determined by sedimentation velocity analysis using SEDANAL (4).

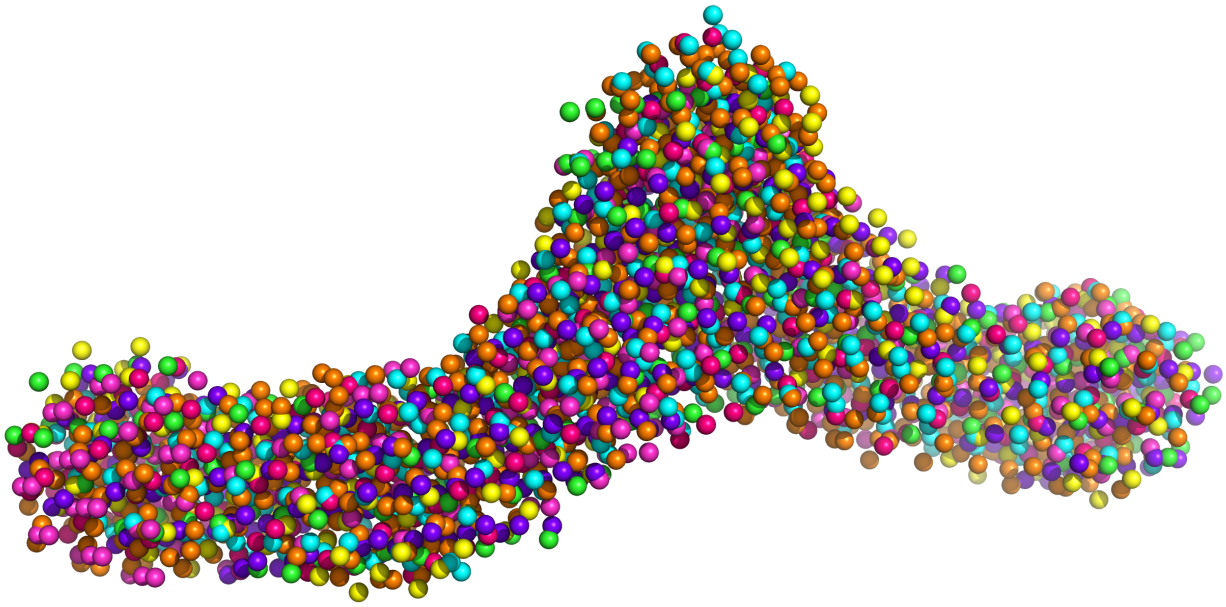

Figure S5. Superposition of *ab initio* structural models of VAI. *Ab initio* structural models were constructed using DAMMIF (5) for eight independent SAXS data sets collected at 1, 2 and 4 mg/ml VAI in the absence and presence of Mg^{2+}. For each structure, 25 simulated annealing runs were performed and the resulting models were superimposed, averaged and filtered using DAMAVER (6). The resulting dummy-atom models were superimposed using SUPCOMB (7) and are depicted as beads of different colors. The maximal normalized spatial discrepancy (NSD) within the group is 0.536.

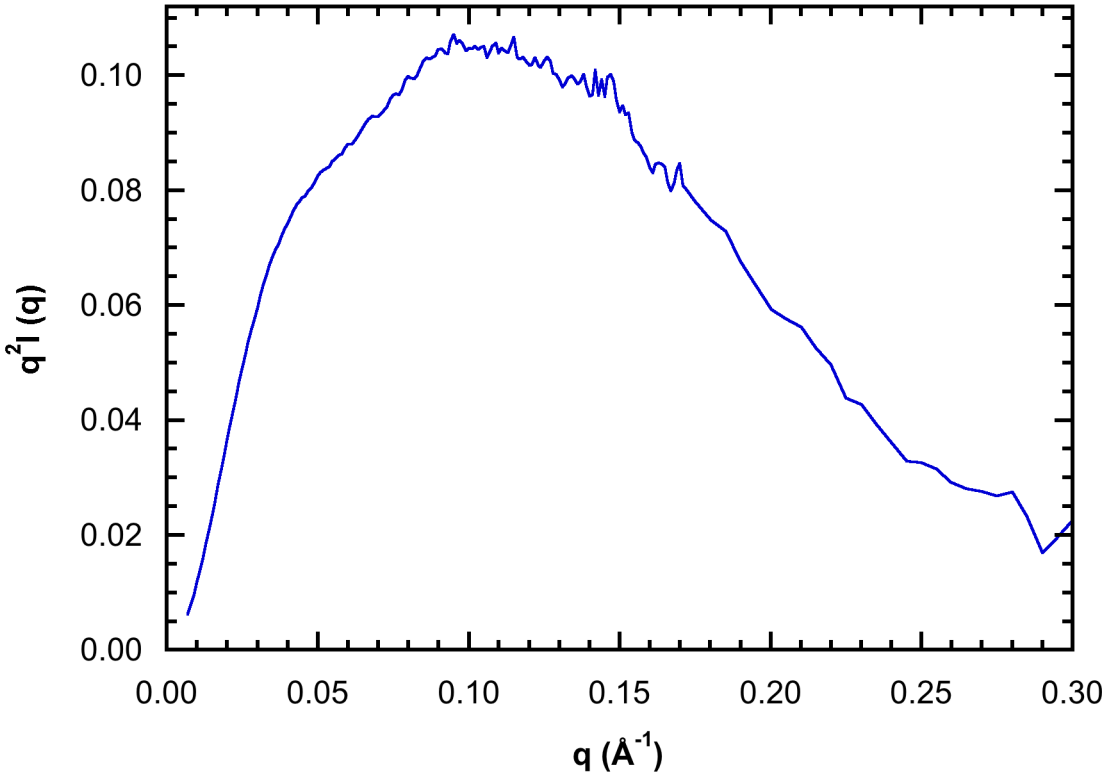

Figure S6. Kratky plot. Scattering data for 2 mg/ml VAI + Mg^{2+} weighted by $q^{2.}$ The plot exhibits a clear maximum and decrease at high *q*, as predicted for a well-ordered macromolecule.

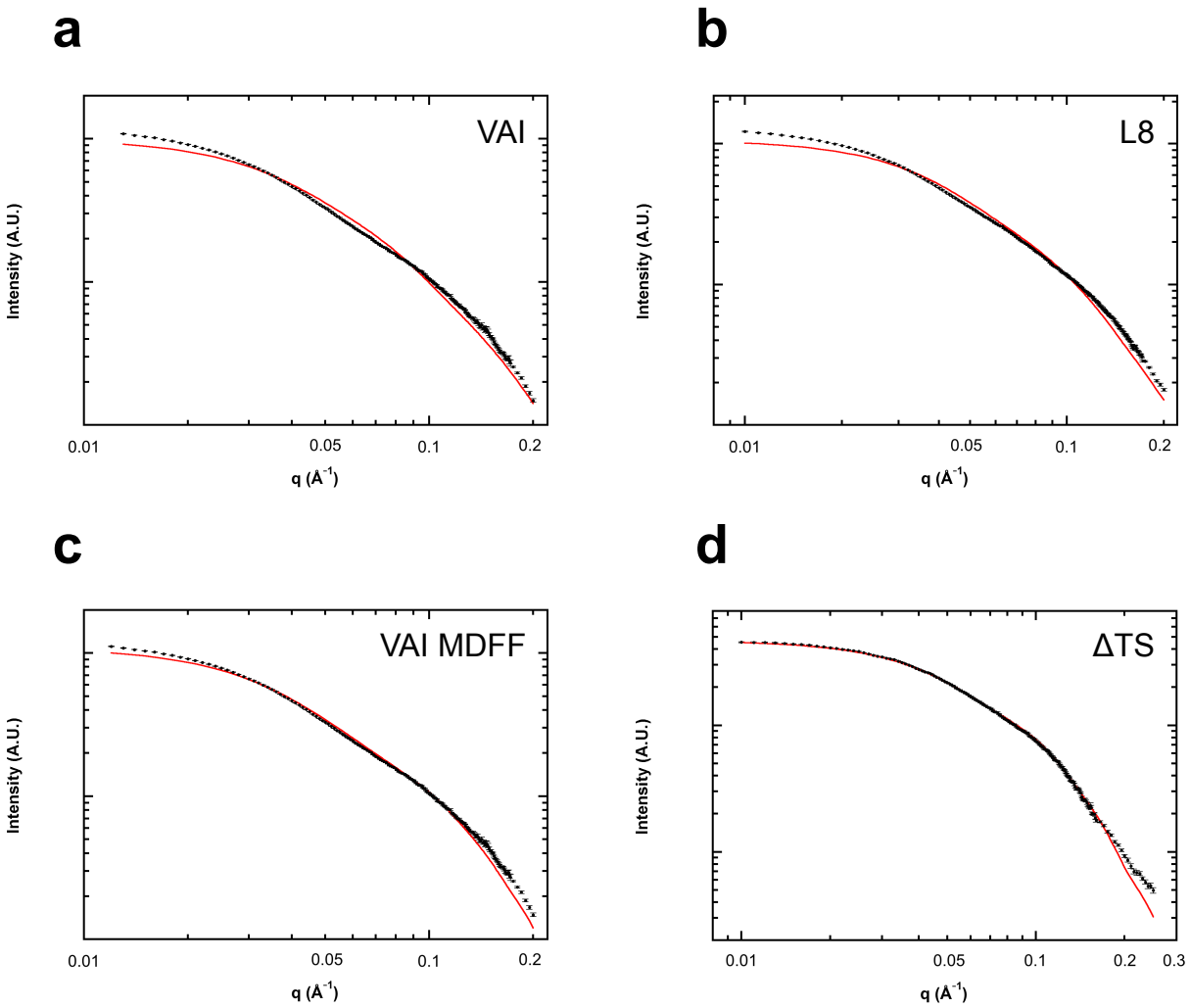

Figure S7. Predicted scattering of atomic models. Scattering curves (red lines) were calculated from the atomic models using CRYSOL(8) and superimposed on the experimental data (black points). a) VAI, b) L8, c) VAI model refined using MDFF (9), d) ΔTS. The reduced χ^2 values are 22.34 (VAI), 21.57 (L8), 11.56 (VAI refined using MDFF) and 3.27 (ΔTS).

Table S1. Parameters derived from SAXS analysis of VAI.

RNA	Conc. (mg/ml)	R_g, Guinier (Å)[a]	R_g, p(r) (Å)[b]	Dmax (Å)[c]	Porod Volume ($Å^3$)[d]
WT	1.0	44.6 ± 0.8	46.4 ± 0.1	160	84,000
WT	2.0	44.8 ± 1.0	46.3 ± 0.1	160	76,700
WT	4.0	42.5 ± 0.7	44.5 ± 0.1	160	71,300
WT + Mg^{2+}	1.0	45.9 ± 0.2	47.1 ± 0.1	160	70,900
WT + Mg^{2+}	2.0	45.1 ± 0.1	47.0 ± 0.1	160	73,500
WT + Mg^{2+}	4.0	45.9 ± 0.1	47.3 ± 0.1	160	75,100
L8 + Mg^{2+}	2.0	45.9 ± 0.7	48.4 ± 0.1	160	71,500
ΔTS + Mg^{2+}	2.0	32.7 ± 1.1	33.1 ± 0.1	110	39,700

[a]Radius of gyration obtained by Guinier analysis.

[b]Radius of gyration obtained from the second moment of the p(r) distribution using GNOM (10).

[c]Maximum dimension. D_{Max} was determined by the minimum of X^2 as this parameter was incremented using GNOM (10).

[d]The Porod volume was determined with DATPOROD (11).

Supporting References

1. Schuck, P. 2000. Size-distribution analysis of macromolecules by sedimentation velocity ultracentrifugation and lamm equation modeling. Biophys J. 78: 1606–1619.

2. Launer-Felty, K., C.J. Wong, A.M. Wahid, G.L. Conn, and J.L. Cole. 2010. Magnesium-dependent interaction of PKR with adenovirus VAI. J Mol Biol. 402: 638–644.

3. Das, R., A. Laederach, S.M. Pearlman, D. Herschlag, and R.B. Altman. 2005. SAFA: semi-automated footprinting analysis software for high-throughput quantification of nucleic acid footprinting experiments. RNA. 11: 344–354.

4. Stafford, W.F., and P.J. Sherwood. 2004. Analysis of heterologous interacting systems by sedimentation velocity: curve fitting algorithms for estimation of sedimentation coefficients, equilibrium and kinetic constants. Biophys Chem. 108: 231–243.

5. Franke, D., and D. Svergun. 2009. DAMMIF, a program for rapid ab-initio shape determination in small-angle scattering. J Appl Crystallogr. 42: 342–346.

6. Volkov, V., and D. Svergun. 2003. Uniqueness of ab initio shape determination in small-angle scattering. J Appl Crystallogr. 36: 860–864.

7. Kozin, M.B., and D.I. Svergun. 2001. Automated matching of high-and low-resolution structural models. J Appl Crystallogr. 34: 33–41.

8. Svergun, D., C. Barberato, and M. Koch. 1995. CRYSOL-a program to evaluate X-ray solution scattering of biological macromolecules from atomic coordinates. J Appl Crystallogr. 28: 768–773.

9. Trabuco, L.G., E. Villa, K. Mitra, J. Frank, and K. Schulten. 2008. Flexible fitting of atomic structures into electron microscopy maps using molecular dynamics. Structure/Folding and Design. 16: 673–683.

10. Semenyuk, A.V., and D.I. Svergun. 1991. GNOM – a program package for small-angle scattering data processing. J Appl Crystallogr. 24: 537–540.

11. Petoukhov, M.V., D. Franke, A.V. Shkumatov, G. Tria, A.G. Kikhney, et al. 2012. New developments in the ATSASprogram package for small-angle scattering data analysis. J Appl Crystallogr. 45: 342–350.